Fabrication and testing of the first 8.4 m off-axis segment for the Giant Magellan Telescope

H. M. Martin[a], R. G. Allen[a], J. H. Burge[a,b], D. W. Kim[b], J. S. Kingsley[a], M. T. Tuell[a], S. C. West[a], C. Zhao[b] and T. Zobrist[b]

[a]Steward Observatory, University of Arizona, Tucson, AZ 85721, USA
[b]College of Optical Sciences, University of Arizona, Tucson, AZ 85721, USA

ABSTRACT

The primary mirror of the Giant Magellan Telescope consists of seven 8.4 m segments which are borosilicate honeycomb sandwich mirrors. Fabrication and testing of the off-axis segments is challenging and has led to a number of innovations in manufacturing technology. The polishing system includes an actively stressed lap that follows the shape of the aspheric surface, used for large-scale figuring and smoothing, and a passive "rigid conformal lap" for small-scale figuring and smoothing. Four independent measurement systems support all stages of fabrication and provide redundant measurements of all critical parameters including mirror figure, radius of curvature, off-axis distance and clocking. The first measurement uses a laser tracker to scan the surface, with external references to compensate for rigid body displacements and refractive index variations. The main optical test is a full-aperture interferometric measurement, but it requires an asymmetric null corrector with three elements, including a 3.75 m mirror and a computer-generated hologram, to compensate for the surface's 14 mm departure from the best-fit sphere. Two additional optical tests measure large-scale and small-scale structure, with some overlap. Together these measurements provide high confidence that the segments meet all requirements.

Keywords: telescopes, optical fabrication, optical testing, off-axis, aspheres, active optics

1. INTRODUCTION

The unique design of the Giant Magellan Telescope (GMT)[1],[2] makes use of the largest segments that can be made. The 8.4 m honeycomb-sandwich mirror segments, combined with matching 1.06 m secondary mirror segments, guarantee smooth wavefronts over the largest possible subapertures and minimize the degrees of freedom that will be controlled actively. The University of Arizona has transformed its Mirror Lab into a production facility for the seven GMT segments (plus one spare). The Mirror Lab houses the furnace for casting the lightweight mirrors, a three-axis generator, and a two-spindle computer-controlled polisher, all sized for 8.4 m mirrors. The Lab recently installed a 28 m test tower that contains four powerful test systems for the GMT segments. The measurements guide all stages of fabrication and guarantee that the segments meet all requirements. The set of tests emphasizes redundant measurements of all critical parameters.

This paper gives an overview of the fabrication and measurement of the first GMT segment. Previous papers describe the early stages of fabrication[3],[4] and present some of the measurement systems[5]-[10]. More detailed papers on the measurements are presented in this conference[11]-[13]. Section 2 of this paper summarizes the accuracy requirements, which are unique in some respects. Section 3 describes the fabrication process and Section 4 the measurements. Section 5 presents the current status of the first segment.

2. ACCURACY REQUIREMENTS

Accuracy requirements for the GMT segments were described in a previous paper[4] and will be summarized here. Requirements at small and medium spatial scales are similar to those for any telescope mirror. On large scales, there are several requirements and methods of dealing with requirements that are unique to off-axis segments. One difference with respect to conventional telescope optics is that the radius of curvature must be controlled to high accuracy in order to make the segments form a single 25 m surface. Focus is measured and controlled like any other low-order aberration. Another difference is related to the difficulty of measuring certain low-order aberrations in the lab because of the lack of symmetry in the segment surface and the test optics. The off-axis surface contains 13 mm p-v astigmatism. In the main optical test, this astigmatism is introduced into the test wavefront by a non-axisymmetric set of

Modern Technologies in Space- and Ground-based Telescopes and Instrumentation, edited by Eli Atad-Ettedgui, Dietrich Lemke, Proc. of SPIE Vol. 7739, 77390A · © 2010 SPIE · CCC code: 0277-786X/10/$18 · doi: 10.1117/12.857494

optics (the null corrector). The accuracy we expect to achieve in the test wavefront, roughly 2 μm p-v, is not adequate to support seeing-limited observations. We can, however, guarantee that the mirrors will meet all requirements in the telescope by anticipating the use of active optics.

Traditionally, active optics involves bending the mirror to the desired shape based on wavefront measurements in the telescope. These wavefront measurements use the telescope's natural geometry with starlight to obtain much better large-scale accuracy than a lab measurement using a null corrector. For off-axis segments, in addition to the bending degrees of freedom, alignment of the segment—motion along the parent surface—provides valuable degrees of freedom. Table 1 shows that displacements of 1 mm can compensate for significant magnitudes of focus, astigmatism and coma. Alignment has only two degrees of freedom—off-axis distance and clocking—so bending is also required to eliminate these and other aberrations. But the aberrations that are most sensitive to alignment are the same aberrations that have the largest uncertainty in the lab measurements, so alignment is an important part of the active optics system. The best approach is to find the combination of alignment and bending that minimizes both the bending forces and the residual surface error.

Table 1. Sensitivity of low-order aberrations to off-axis distance and clocking (rotation about the segments' mechanical center). Clocking by 50″ causes a point at the edge to move by 1 mm. Values differ slightly from those listed in Ref. [4].

aberration	rms surface error (nm)	
	1 mm change in off-axis distance	50" rotation
focus	810	
astigmatism	510	1240
coma	34	160

Table 2 gives the relationship between surface error and bending force for several low-order aberrations. It lists the amount of each aberration that can be induced with 10 N rms force over the 165 active supports, assuming the forces are optimized to match that particular aberration. It also lists the residual surface error, i. e. the difference between the actual shape change and the desired aberration, again for 10 N rms force. The forces are applied as a set of bending modes, starting with the softest mode and going to increasingly stiffer modes. Using more modes gives a better match to the desired aberration—it reduces the residual error—but requires larger forces. Using fewer modes requires less force for a given amplitude of the aberration, but leaves larger residual errors. Table 2 reflects a reasonable balance between forces and residual errors, but other combinations could be used.

Table 2. Sensitivity of five low-order aberrations to bending force. Values differ slightly from those listed in Ref. [4].

aberration	amplitude for 10 N rms force (nm rms surface)	residual error for 10 N rms force (nm rms surface)
focus	320	15
astigmatism	920	15
coma	77	10
trefoil	210	8
spherical aberration	28	7

When we measure the segment's figure in the lab, the data processing includes a simulation of active optics exactly as it will be done in the telescope. The simulation includes both alignment and bending of the segment. The two alignment degrees of freedom are optimized so the residual aberrations can be bent out with a minimum set of bending

forces. We keep track of the off-axis and clocking displacements, the bending forces, and the residual surface error due to imperfect bending. Uncertainties in the lab measurements are handled in the same way. For example, the principal optical test described in Section 4.3 involves a large number of parameters that will have errors that cause astigmatism and other low-order aberrations. We assign an uncertainty to each parameter, calculate the resulting aberrations, simulate the active optics correction, and record the resulting uncertainty in off-axis distance, clocking angle, bending forces, and residual error after bending. The uncertainties due to all parameters are added in quadrature to give the net uncertainty in the optical test.

The tolerance analysis for the optical test shows that the uncertainties in off-axis distance and clocking angle are within their specifications (2 mm and 50″). We allocate 30 N rms force over the 165 active supports to bend out errors due to the optical test. We allocate an additional 30 N rms to bend out low-order aberrations in the measured figure that we choose not to polish out, and add these forces in quadrature to give a net bending force of 42 N rms. This is a small fraction of the average support force of 1070 N at zenith pointing.

The figure error after simulated active optics compensation must satisfy a specification given as a structure function (mean square wavefront difference between points in the aperture as a function of their separation). The form is similar to the power-law for wavefront errors caused by the atmosphere, with the amplitude of errors defined by the coherence length r_0 = 92 cm for λ = 500 nm, corresponding to an image size of 0.11″ FWHM. The specification is tightened on large scales in a way that corresponds to the removal of tilt by active guiding, and relaxed on small scales to allow a small fraction of light to be scattered outside the core of the image. Table 3 summarizes the specifications and goals for figure and geometry.

Table 3. Optical specifications and goals for the first GMT segment

parameter	specification	goal
geometry		
radius of curvature *R*	36,000.0 ± 1.0 mm	± 0.3 mm
measurement accuracy for *R*	± 0.5 mm	± 0.3 mm
conic constant *k*	-0.998286	
off-axis distance	8710 ± 2 mm	± 1 mm
clocking angle	± 50 arcseconds	
figure (structure function, λ = 500 nm)		
clear aperture	8.365 m	
coherence length r_0	91.9 cm	
scattering loss	< 2.0%	< 1.5%

3. FABRICATION

The early stages of fabrication—casting, generating, and loose-abrasive grinding—have been described in previous papers.[3],[4] We are currently polishing and figuring the segment. Most of the work is done with the 1.2 m stressed lap shown in Figure 1. This lap, designed for large-scale figuring and smoothing of highly aspheric surfaces such as the GMT segments, bends actively to match the local curvature of the surface. It is relatively stiff so it provides figuring on large scales and smoothing on smaller scales. For figuring of medium- and small-scale structure we use a new tool known as a rigid conformal (RC) lap.[14] It contains a layer of non-linear visco-elastic fluid that is stiff on short timescales and compliant through flow on long timescales, and represents a different way to achieve smoothing on highly aspheric surfaces. We have recently used a 27 cm RC lap with an orbital motion as shown in Figure 2.

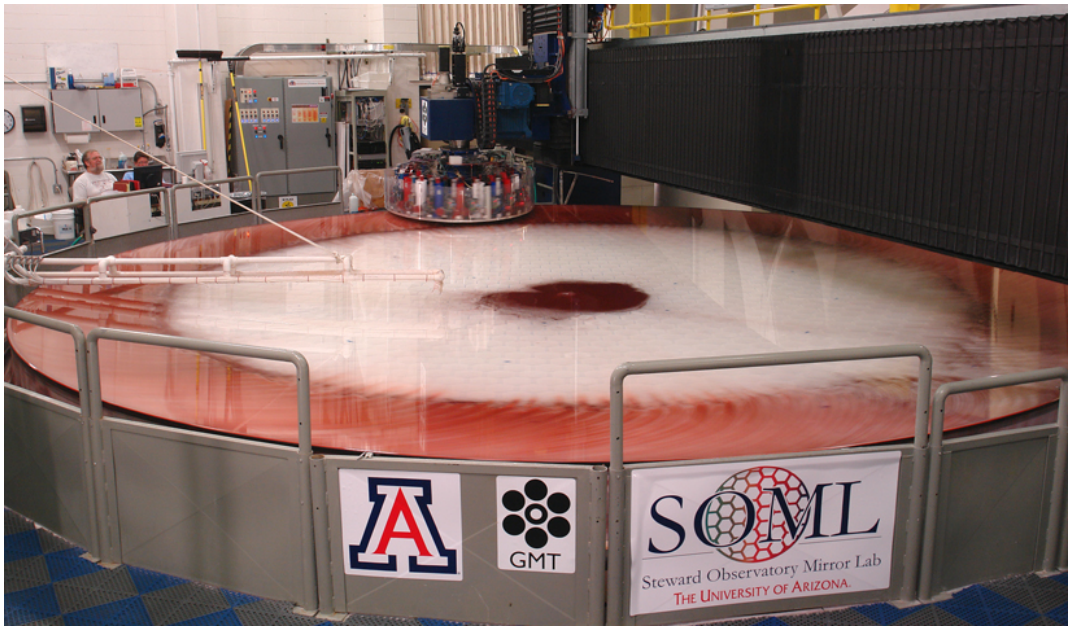

Figure 1. First GMT segment being polished with a 1.2 m stressed lap. Photo by Ray Bertram, Steward Observatory

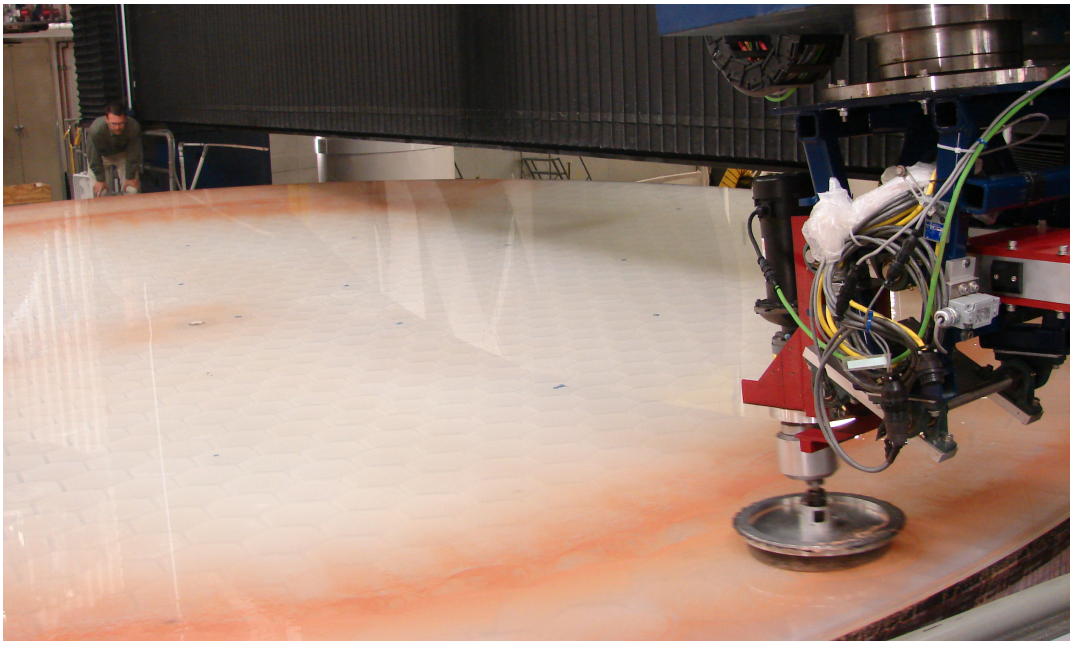

Figure 2. A 27 cm RC lap is used with an orbital polisher for local figuring.

To date we have used the RC lap in a simple mode with uniform dwell over finite extents in both radius and azimuth. We are in the process of implementing more sophisticated control and modeling with variable dwell time optimized to reduce the measured figure error. This technique will be used with the stressed lap as well as the RC lap. The optimization of dwell time as a function of position is performed simultaneously for multiple tools, giving the best combination of strokes over all the available tools.[15] The different tools will be used in sequence, but the optimization of dwells is based on the combination of all tools. This is expected to result in faster convergence and less small-scale residual error than a sequential optimization with a larger tool followed by smaller tools.

4. MEASUREMENT

4.1 Overview

Four independent measurements have been implemented for the GMT segments. They were designed to satisfy the following high-level requirements:

1. Measure large-scale errors accurately enough that they can be corrected in the telescope with a combination of segment alignment within the specified position tolerance and bending using forces within the specified limit.
2. Measure small-scale errors to an accuracy that represents a small fraction of the specification for figure errors.
3. Measure the segment's geometry (radius of curvature, off-axis distance, and clocking angle) within the specified tolerances.
4. Include enough redundancy that a mistake in implementing one of the tests would be caught by another test.
5. Support all three stages of fabrication: generating, loose-abrasive grinding and polishing.

All four test systems are installed in the 28 m test tower. The tower is sized to accommodate the main interferometric optical test, which includes as part of its null corrector a 3.75 m spherical mirror located at the top of the tower.

4.2 Laser Tracker Plus system

The first measurement that was implemented uses a laser tracker to scan the surface.[10] This test guides the generating, loose-abrasive grinding, and initial polishing. It also measures radius of curvature and astigmatism to accuracies roughly equal to the segment specifications and thereby serves as a valuable confirmation of the optical tests.

The laser tracker combines a distance-measuring interferometer (DMI) with angle encoders and a pointing servo to track a moving retroreflector and measure its position in 3 dimensions. The distance measurement is sensitive to displacements of a small fraction of a micron, while the angular measurements are accurate to about 1 μrad rms over the range of angles subtended by the segment. This combination gives a surprisingly accurate measurement of the mirror surface provided the line of sight is roughly normal to the surface, i. e. the laser tracker is near the mirror's center of curvature. In this case the DMI measures the surface displacement while the angle encoders are used only to define the location on the mirror.

For the GMT segments, with R = 36 m, we don't have access to the center of curvature. The laser tracker is located 22 m above the mirror. Because of the non-normal incidence, we are sensitive to angular errors in the laser tracker measurements. The ratio of apparent surface error to angular error is 1.6 μm/μrad at the outer edge of the segment.

The system used at the Mirror Lab is enhanced in several ways, hence the name Laser Tracker Plus. In terms of accuracy, the most important enhancement is a set of reference DMIs mounted on the laser tracker platform and staring at fixed retroreflectors on the edge of the segment. They monitor rigid-body motion of the segment relative to the laser tracker platform, as well as large-scale refractive index variations that look like rigid-body motion. We typically see several microns of rigid-body motion during a scan, but this is compensated by the reference system.

Laser Tracker Plus includes an automated system to scan the retroreflector over the surface. The standard retroreflector for a laser tracker is mounted in a steel ball. In our system the ball is held by a puck with 4 strings attached. Motors control the string lengths and tensions to drag the puck over the surface. For use on the polished surface, we use a pneumatic puck with air bearings and a slow valve that sets the ball gently down on the surface at each measurement point. The system measures about 250 points at 0.5 m spacing in about 45 minutes, with no operator present. We have also found it valuable to make high-density radial scans at the edge of the mirror.

4.3 Principal optical test

The principal optical test for the GMT segments is a full-aperture interferometric measurement that uses a large multi-element null corrector to transform the interferometer's spherical wavefront into the asymmetric template wavefront that matches the ideal segment surface.[5] This test will measure all aspects of mirror figure and geometry to

an accuracy consistent with the specifications listed in Table 3. Two optical slope tests described in the following subsections will give independent confirmation of the accuracy of the principal test, on different spatial scales.

Figure 3 shows a model of the full test. The null corrector comprises a computer-generated hologram (CGH), a 0.76 m spherical mirror and a 3.75 m sphere. This is an asymmetric null corrector for the off-axis segment rather than a symmetric system that could test the 25 m parent. Figure 4 shows the shaping of the wavefront by the 3 elements of the null corrector. The 3.75 m sphere introduces a little more than half the astigmatism and most of the coma, the 0.76 m sphere introduces the rest of the low-order aberrations, and the hologram produces the remaining high-order aspheric departure. The figure error in the 3.75 m sphere can't be neglected, so we measure it in real time (simultaneous with the measurement of the GMT segment) from its center of curvature and correct for its figure error. Figure 5 shows the test optics installed in the test tower.

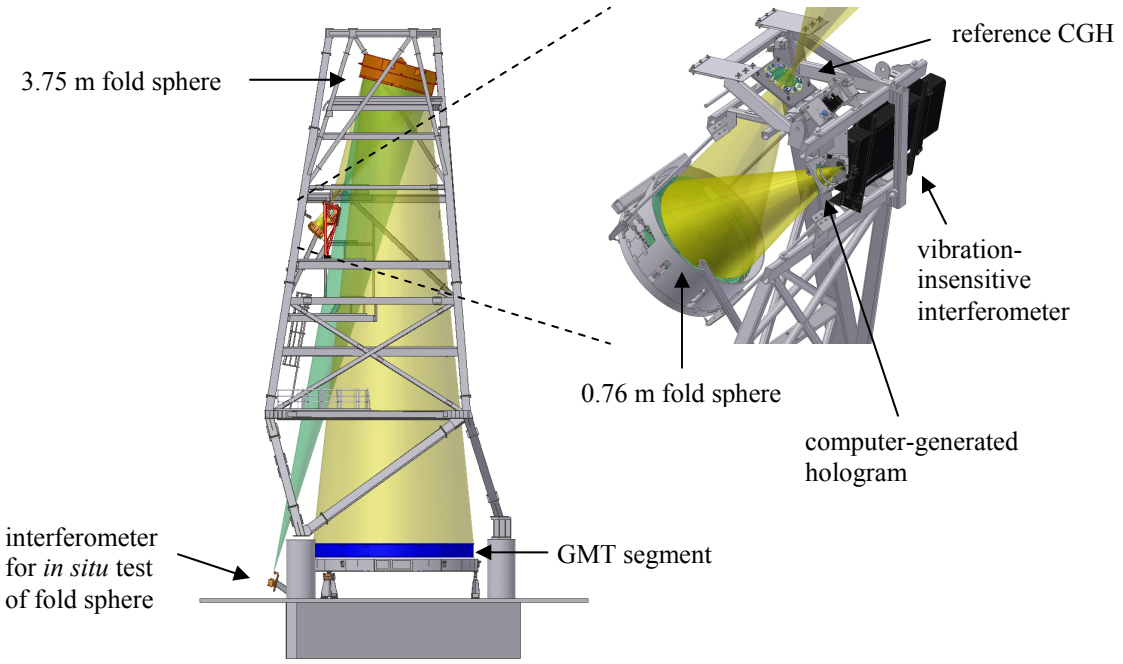

Figure 3. Model of the principal optical test for the GMT off-axis segments, in the 28 m test tower. At right is a blow-up of the interferometer and first two elements of the null corrector. The reference CGH is inserted for alignment of the test system but removed for the measurement of the GMT segment. Gold light cones represent the measurement of the GMT segment, while the aqua cone in the full model at left represents a simultaneous measurement of the 3.75 m fold sphere.

Alignment tolerances for this optical test are challenging, in part because of the lack of symmetry. We developed techniques based on CGHs, laser trackers and a point-source microscope to align the interferometer and first two elements of the null corrector to accuracy on the order of 10 μm, and the full system including the GMT segment to the order of 100 μm.[11] The most challenging aspect of the large-scale alignment is determining the orientations of the smaller elements relative to the rest of the system. We do this by introducing a temporary reference CGH at the intermediate focus between the two spheres.[5] (This is a blurry focus with 6 mm of aberration; see Figure 4.) The reference hologram is designed to return a null wavefront to the interferometer, so the hologram can be aligned to match the wavefront at the intermediate focus. With this information, we can ignore the individual components and align the large sphere and GMT segment to the wavefront at the intermediate focus. (The alignment of the smaller elements relative to one another is still critical so that we achieve an accurate wavefront.) The reference hologram is written on a glass substrate that contains alignment references, including small flat mirrors that are aligned to match features on the hologram and whose orientations can be measured with the laser tracker. These measurements are tied to laser tracker measurements of the large sphere and GMT segment to determine the relative positions and orientations in all degrees of freedom.

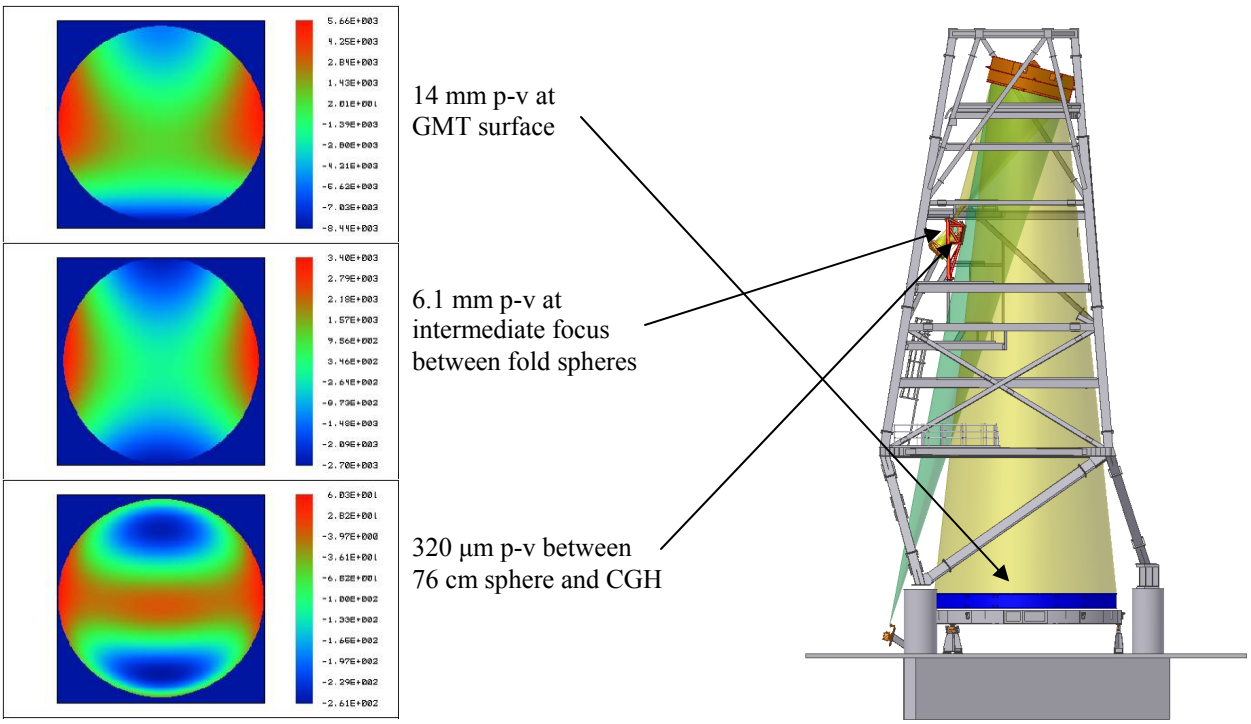

Figure 4. Shaping of the wavefront by the null corrector. The interferometer's spherical wavefront is shaped first by the CGH, then by the 76 cm sphere, and finally by the 3.75 m sphere.

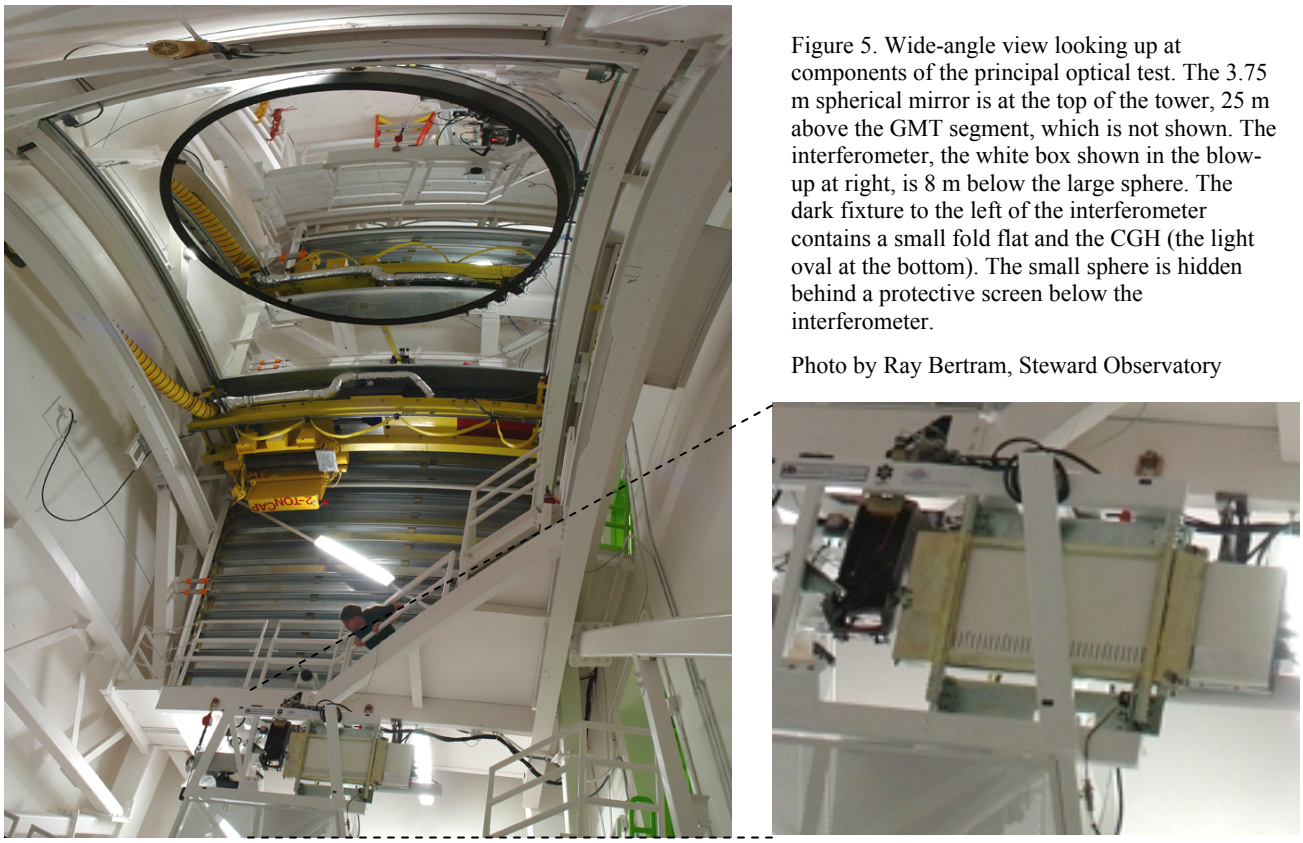

Figure 5. Wide-angle view looking up at components of the principal optical test. The 3.75 m spherical mirror is at the top of the tower, 25 m above the GMT segment, which is not shown. The interferometer, the white box shown in the blow-up at right, is 8 m below the large sphere. The dark fixture to the left of the interferometer contains a small fold flat and the CGH (the light oval at the bottom). The small sphere is hidden behind a protective screen below the interferometer.

Photo by Ray Bertram, Steward Observatory

When we align the system for a test, the last optic to be moved is the GMT segment. It is initially aligned to the 100 μm level based on laser tracker measurements of reference targets at the edge of the mirror, using a 6-axis mechanical positioner. From that point, the only adjustable degrees of freedom are tip and tilt, which are adjusted with sub-micron resolution to null the interference fringes, using highly leveraged pistons in the segment's 3-sector hydraulic support system.

We are still refining the alignment system based on the reference hologram.[11] The first implementation had the flat mirrors bonded to a mounting plate and the hologram kinematically mounted on that plate. The kinematic mounting was not repeatable enough in orientation. We are in the process of installing a second-generation reference hologram with the flat mirrors bonded directly to the hologram substrate so we do not rely on repeatable mounting. This is a significant improvement and is expected to meet all requirements.

We have performed a thorough analysis of uncertainties in the principal test. The analysis shows that the test will meet all requirements for figure and geometry. The radius of curvature, off-axis distance and low-order aberrations will be measured to sufficient accuracy that any errors can be corrected at the telescope with the active optics system, using acceptable displacements and forces. The remaining figure errors will be measured to an accuracy that uses a small fraction of the figure specification, leaving almost the entire specification available for measured figure error. But it would be too risky to rely on a single test, especially one of this complexity. We have developed two other tests that together verify the accuracy of the principal test on all spatial scales. They are described in the following subsections.

4.4 Scanning pentaprism test

If a mistake were made in implementing the principal test, it would most likely be in alignment and would affect only low-order aberrations. We developed a scanning pentaprism test to measure the low-order aberrations, including focus, to accuracies consistent with the segment specifications.[6],[7] The pentaprism test, shown in Figure 6, measures slope errors in one-dimensional scans across different diameters of the segment. It synthesizes a collimated wavefront by scanning a 45 mm diameter beam across the segment. This beam is brought to a focus at the segment focus, where a detector measures the position of the spot. Displacement of the spot at the detector is proportional to the slope error on the segment surface. For a parabolic segment, this is a null test in that the spot should not move as the beam is scanned across the surface. For the slightly ellipsoidal GMT segments (k = -0.99826), we compensate for the expected spot motion.

The pentaprism rail shown in Figure 6 lies in a plane perpendicular to the optical axis of the GMT parent. A beam projector at one end of the rail sends collimated light along the rail. About half the light is deflected down, parallel to the optical axis, by a pentaprism beamsplitter, and the rest is deflected down by a second pentaprism. Both deflected beams form spots on the detector at the focus. The pentaprism beamsplitter is stationary while the second pentaprism is scanned along the rail across the diameter of the segment. The pentaprisms deflect the beam by a fixed angle of about 90°. In the plane defined by the rail and the optical axis, this angle is independent of small rotations of the pentaprisms. The angle of deflection within this plane, and the corresponding spot displacement at the detector, define the in-scan direction of spot motion. In-scan spot motion depends only on the local slope of the mirror surface and on a number of system misalignments that affect both spots equally (tilt of the beam projector, tilt of the GMT segment, and motion of the detector assembly). By measuring differential motion between the two spots, we eliminate the effects of system misalignments and measure only the local slope of the mirror surface as a function of position along the scan. The deflection by the pentaprism in the plane perpendicular to the rail is not well controlled, so we ignore spot motion perpendicular to the in-scan direction.

The pentaprism rail is deployed from the side of the test tower, and removed from the light path for the other measurements. The rail rotates around a bearing whose axis is parallel to the optical axis and intersects near the center of the segment, so the system can scan across any diameter of the segment. The in-scan component of surface slopes is always approximately in the radial direction, along a diameter of the segment. A basic measurement consisting of 4 scans at 45° intervals determines the low-order aberrations through spherical and high-order astigmatism, but more scans can be used to obtain more detailed information. Even with a limited number of scans, the test gives valuable information on small-scale structure in the radial direction as well as low-order aberrations.

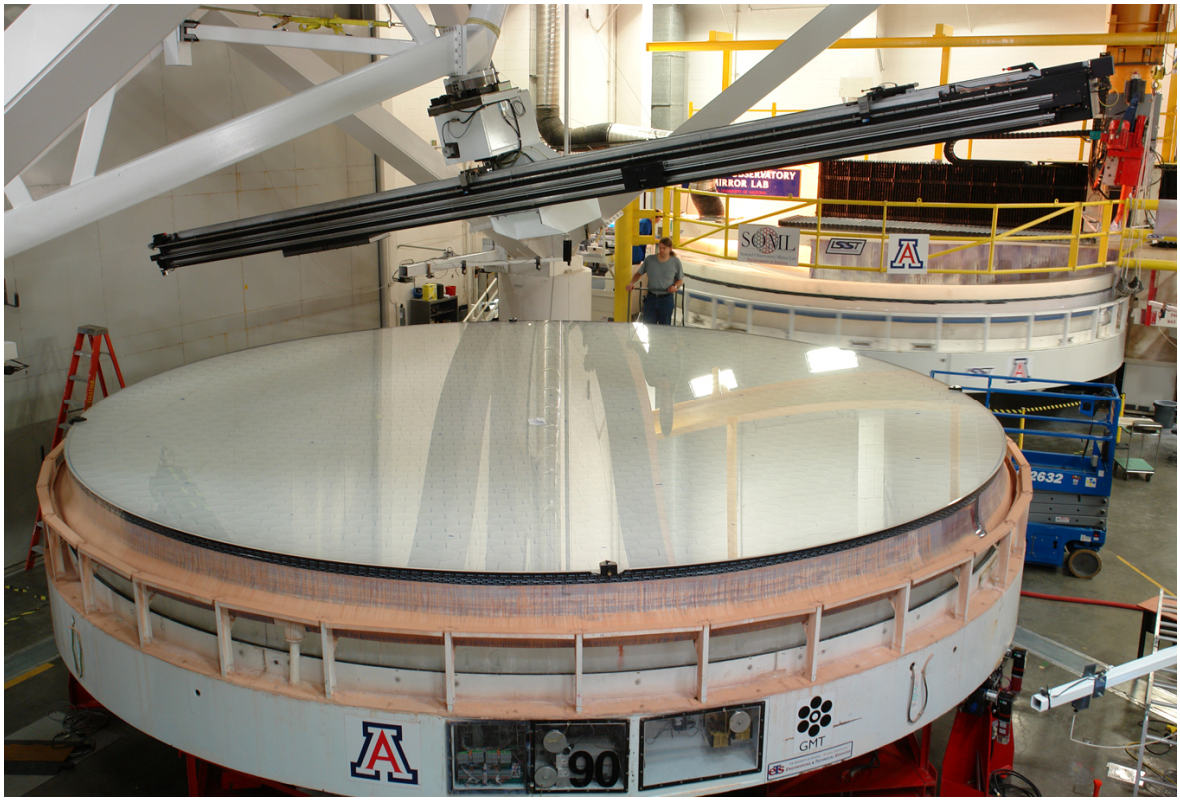

Figure 6. GMT segment with the 8.4 m pentaprism rail. Not shown is the pentaprism detector, which is at the segment focus 18.5 m above the segment and 4.5 m to the right of the segment center. In the background is the LSST combined primary-tertiary mirror. Photo by Ray Bertram, Steward Observatory

Wavefront slope errors due to the test are controlled to about 1 μrad rms. By fitting polynomials to the measured slopes, we can measure focus, astigmatism, coma, trefoil and spherical aberration to about the same accuracy achieved by the principal test, sufficient to satisfy the segment specifications. Combining these aberrations with laser tracker measurements of the position of the segment and detector, we expect to use the pentaprism test to determine the segment's focal length and off-axis distance to better than 0.25 mm.

4.5 SCOTS slope test

The main purpose of the pentaprism test is to provide an independent measurement of low-order aberrations and segment geometry. It also measures small-scale structure, but only slopes in the radial direction along the scan lines. A different slope test, the Software Configurable Optical Test System (SCOTS), was developed to measure small- and mid-scale structure on highly aspheric surfaces.[16] Applied to the GMT segment, the SCOTS test is complementary to the pentaprism test. Together these tests provide independent confirmation of the principal optical test.

The SCOTS test requires minimal hardware: a computer monitor and a camera. (This can be as simple as a laptop with a built-in camera.) A pattern is displayed on the monitor, and its image through the mirror under test is recorded with the camera. Knowledge of the coordinates of the pattern on the monitor, and the coordinates of its reflection from the mirror, determines the slope at each position on the mirror surface. More precisely, the pattern is displayed as a series of lines whose images are recorded separately by the camera. This technique resolves ambiguities caused by a single pixel on the monitor having multiple images through the mirror under test.

For the GMT segment, the SCOTS hardware is located near the intermediate focus between the two spherical mirrors of the principal test. It uses the 3.75 m sphere to illuminate the GMT surface. The overall geometry of the test is not controlled well enough to measure low-order aberrations to a meaningful accuracy. Currently we ignore 21 Zernike polynomials. The remaining information contains structure on scales from about 2 m down to 1 cm.

5. CURRENT STATUS

Manufacture of the first GMT segment has been a parallel effort in figuring the mirror and developing the test systems. The Laser Tracker Plus system has met its goals and guided the figuring through loose-abrasive grinding and initial polishing. The figuring is now being guided by the principal optical test and the SCOTS test. Neither of these tests is in its final configuration, but both are close. We are in the process of improving the alignment of the principal test and expect it to meet its specifications at the completion of the upgrade. The pentaprism test hardware has recently been completed and we are in the process of making and analyzing the first set of measurements.

Figure 7 shows the reduction in figure errors during the first 4 months of 2010. We suspended polishing in May to work on several upgrades to the system including installation of the new reference hologram, and the first pentaprism measurement. Figure 7 shows that a large error in focus, or radius of curvature, has been corrected during the figuring. This error was caused by inadequate thermal control of the segment during early measurements. We have nearly completed the focus correction while reducing the residual error in parallel.

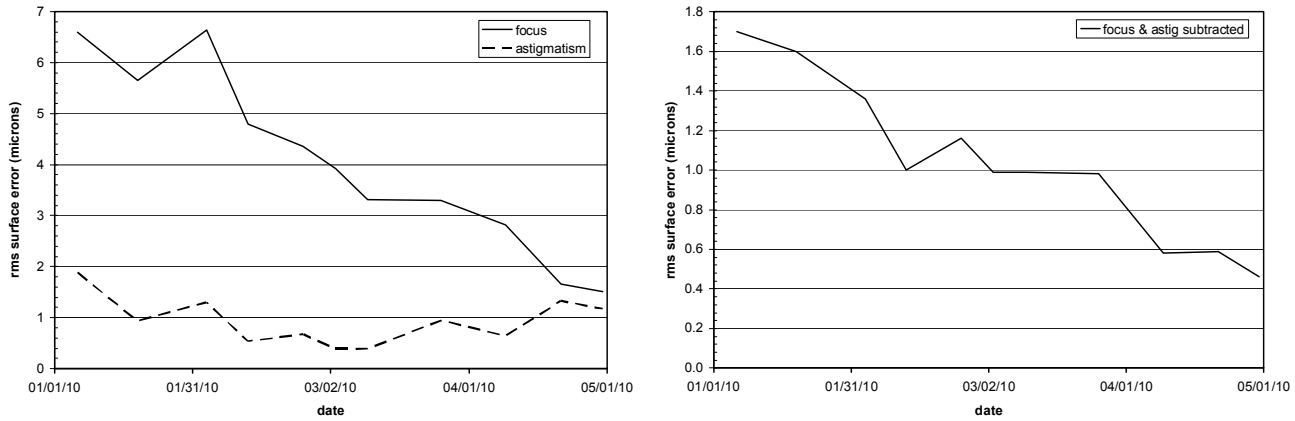

Figure 7. Reduction in figure errors during the first 4 months of 2010, Left: focus and astigmatism. Right: residual error after subtracting focus and astigmatism.

As described in Section 2, focus must be controlled, but both focus and astigmatism have relatively loose tolerances. The focus error of 1.5 μm rms on May 1 is equivalent to an error of -0.86 mm in radius of curvature. This meets the specification but not the goal (Table 3), and in any case it needs to be reduced to allow for uncertainty in the measurements. Only 12 N rms force is needed to bend out 1 μm rms astigmatism. We will continue to reduce both aberrations until the measured amplitudes are roughly 100 nm rms. Some of the inconsistency in the low-order aberrations is probably due to inconsistent alignment of the principal test. We expect to see more consistent results after the alignment upgrade is completed.

Figure 8 shows the segment's surface error as of May 1, 2010. This map is a synthesis of data from the principal optical test (21 Zernike polynomials) and the SCOTS test (everything else). The principal test alone currently loses some data in the outer 20 cm of the segment due to a combination of high fringe density and a temporary lack of vibration isolation. The SCOTS measurement is not affected by these issues and gives an accurate representation of all small-scale and mid-scale structure.

Measurements with the Laser Tracker Plus system are in reasonably good agreement with the principal test. Figure 9 shows the most recent measurements of each, with and without focus and astigmatism. The Laser Tracker Plus map is an 8^{th} degree polynomial fit to the 256 measured points (0.5 m sampling). The differences in focus (1.0 μm rms surface) and astigmatism (0.7 μm rms) are close to the target accuracy for the Laser Tracker Plus, but we expect that small misalignments of the principal test are also contributing significant errors in these aberrations. With these aberrations subtracted, much of the difference is small-scale structure that the Laser Tracker Plus does not resolve.

The SCOTS test is in very good agreement with the principal test. Figure 10 shows the most recent results. Because the SCOTS measurement ignores 21 Zernike polynomials, we subtract the same polynomials from the principal test map shown in Figure 9. Much of the difference is noise in the principal test near the edge of the segment.

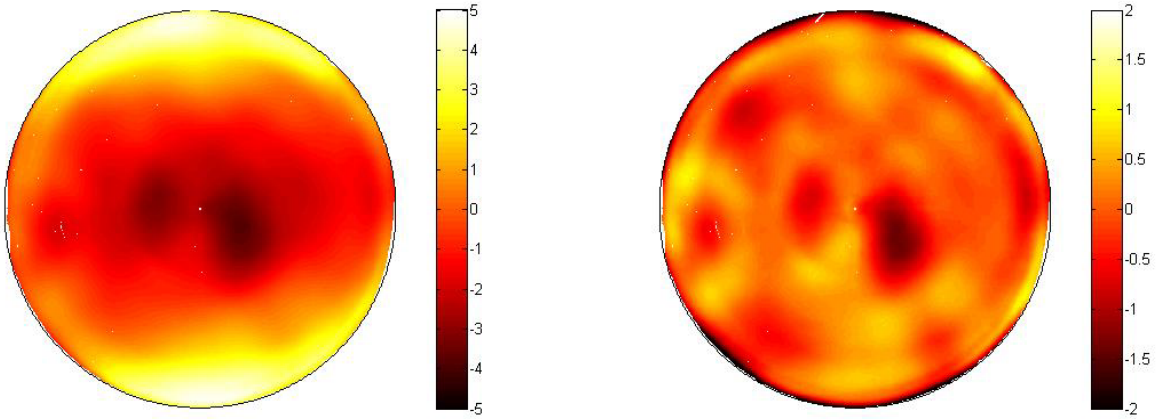

Figure 8. Surface error as of May 1, 2010. The color bar is labeled in microns. The dark circle indicates the edge of the mirror, 8.40 m in diameter.

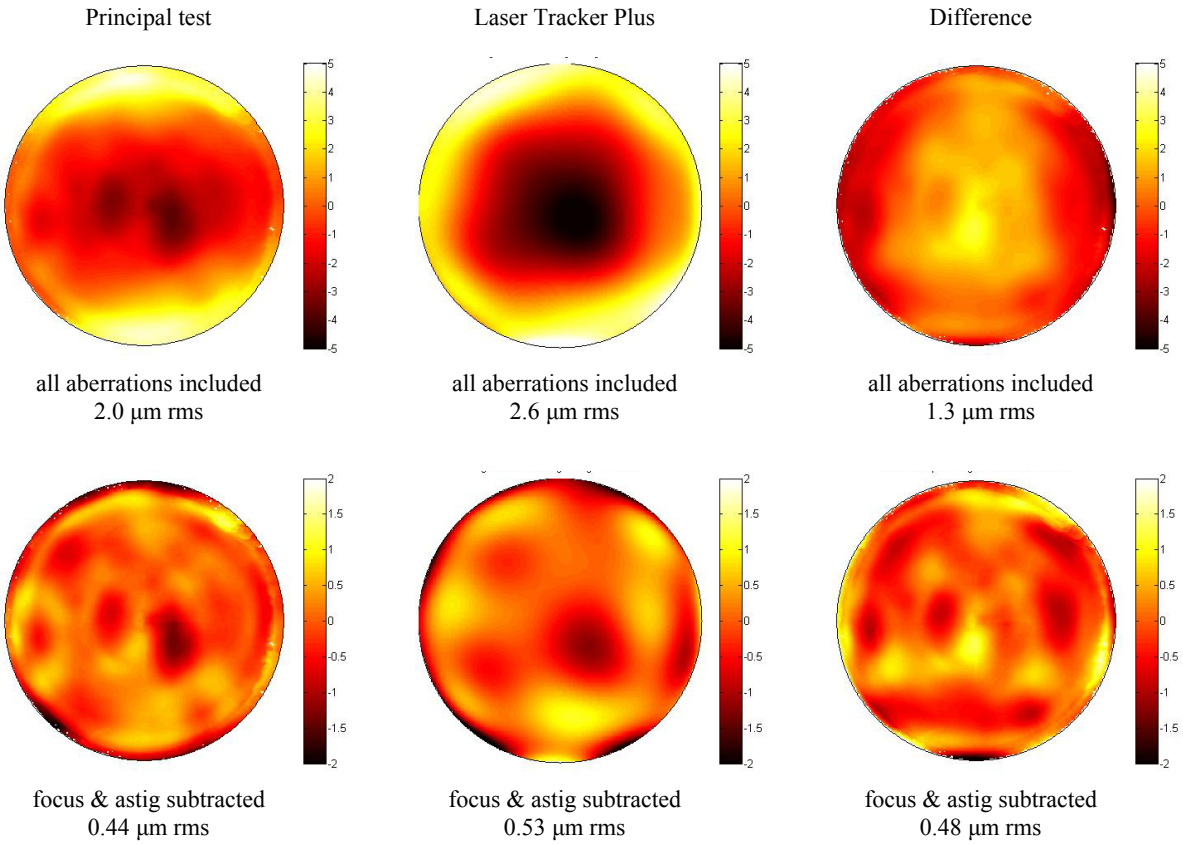

Figure 9. Comparison of measurements with the principal optical test (left) and the Laser Tracker Plus system (center). The two measurements and their difference are shown with no adjustments (top) and with focus and astigmatism subtracted (bottom). Color bars and values listed are surface error.

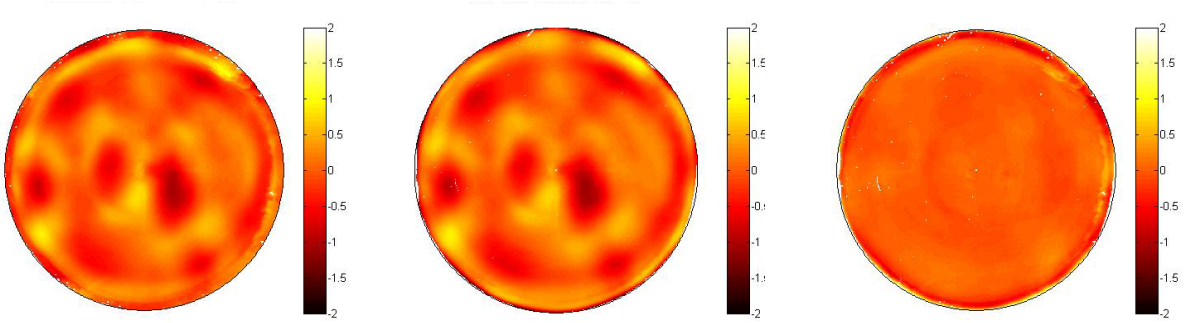

Principal test
21 polynomials subtracted
0.32 μm rms

SCOTS
21 polynomials subtracted
0.35 μm rms

difference
0.16 μm rms

Figure 10. Comparison of measurements with the principal test (left) and SCOTS test (center). For both measurements 21 Zernike polynomials have been subtracted. Color bars and values listed are surface error.

6. SUMMARY

The first GMT segment is nearing completion. The segment's figure is improving steadily. The stressed-lap polishing system has been augmented with a new small-tool computer-controlled polishing capability. Three of the four test systems are in use while the fourth is complete and ready for use in June 2010. The independent measurements agree at the expected levels, although final confirmation of the measurement accuracy will be achieved when the mirror figure is close to its final accuracy. On completion of refinements to the alignment of the principal optical test, and demonstration of the pentaprism test, the Mirror Lab will have in place a complete system for efficient serial production of the remaining GMT segments.

ACKNOWLEDGEMENT

This material is based in part upon work supported by AURA through the National Science Foundation under Scientific Program Order No. 10 as issued for support of the Giant Segmented Mirror Telescope for the United States Astronomical Community, in accordance with Proposal No. AST-0443999 submitted by AURA.

REFERENCES

[1] M. Johns, "Progress on the GMT", *Ground-based and Airborne Telescopes II*, Proc. SPIE 7012, 70121B (2008).

[2] M. Johns, "The Giant Magellan Telescope (GMT)", *Ground-based and Airborne Telescopes*, Proc. SPIE 6267, 626729 (2006).

[3] H. M. Martin, J. R. P. Angel, J. H. Burge, B. Cuerden, W. B. Davison, M. Johns, J. S. Kingsley, L. B. Kot, R. D. Lutz, S. M. Miller, S. A. Shectman, P. A. Strittmatter and C. Zhao, "Design and manufacture of 8.4 m primary mirror segments and supports for the GMT", *Optomechanical Technologies for Astronomy*, Proc. SPIE 6273, 62730E (2006).

[4] H. M. Martin, J. H. Burge, B. Cuerden, W. B. Davison, J. S. Kingsley, W. C. Kittrell, R. D. Lutz, S. M. Miller, C. Zhao and T. Zobrist, "Progress in manufacturing the first 8.4 m off-axis segment for the Giant Magellan Telescope", *Advanced Optical and Mechanical Technologies and Instrumentation*, Proc. SPIE 7018, 70180C (2008).

[5] J. H. Burge, W. Davison, H. M. Martin and C. Zhao, "Development of surface metrology for the Giant Magellan Telescope primary mirror", *Advanced Optical and Mechanical Technologies in Telescopes and Instrumentation*, Proc. SPIE 7018, 701814 (2008).

[6] J. H. Burge, L. B. Kot, H. M. Martin, C. Zhao and T. Zobrist, "Alternate surface measurements for GMT primary mirror segments", *Optomechanical Technologies for Astronomy*, Proc. SPIE 6273, 62732T (2006).

[7] P. Su, J. H. Burge, B. Cuerden and H. M. Martin, "Scanning pentaprism measurements of off-axis aspherics", *Advanced Optical and Mechanical Technologies in Telescopes and Instrumentation*, Proc. SPIE 7018, 70183T (2008).

[8] T. Zobrist, J. H. Burge, W. Davison and H. M. Martin, ”Measurement of large optical surfaces with a laser tracker”, *Advanced Optical and Mechanical Technologies in Telescopes and Instrumentation*, Proc. SPIE 7018, 70183U (2008).
[9] P. Su, J. H. Burge, B. Cuerden, R. G. Allen and H. M. Martin, “Scanning pentaprism measurements of off-axis aspherics II,” *Optical Manufacturing and Testing VIII*, Proc. SPIE 7426, 74260Y (2009).
[10] T. L. Zobrist, J. H. Burge and H. M. Martin, “Laser tracker surface measurements of the 8.4 m GMT primary mirror segment,” *Optical Manufacturing and Testing VIII*, Proc. SPIE 7426, 742613 (2009).
[11] S. C. West, J. H. Burge, B. Cuerden, W. B. Davison, J. Hagen, H. M. Martin, M. T. Tuell and C. Zhao, “Alignment and use of the optical test for the 8.4m off-axis primary mirrors of the Giant Magellan Telescope”, *Modern Technologies in Space- and Ground-based Telescopes and Instrumentation*, Proc. SPIE 7739 (2010).
[12] T. L. Zobrist, J. H. Burge and H. M. Martin, “Accuracy of laser tracker measurements of the GMT 8.4 m off-axis mirror segments”, *Modern Technologies in Space- and Ground-based Telescopes and Instrumentation*, Proc. SPIE 7739 (2010).
[13] R. G. Allen, J. H. Burge, P. Su and H. M. Martin, “Scanning pentaprism test for the GMT 8.4 m off-axis segments”, *Modern Technologies in Space- and Ground-based Telescopes and Instrumentation*, Proc. SPIE 7739 (2010).
[14] D. W. Kim and J. H. Burge, “Rigid conformal polishing tool using non-linear visco-elastic effect”, Opt. Express **18**, 2242-2257 (2010).
[15] D. W. Kim, S. Kim and J. H. Burge, “Non-sequential optimization technique for a computer controlled optical surfacing process using multiple tool influence functions”, Opt. Express **17**, 21850-21866 (2009).
[16] P. Su, R. Parks, J. H. Burge, L. Wang and R. Angel, “SCOTS: A computerized reverse Hartmann test,” submitted to Applied Optics (2010).